Eur Biophys J (2004) 33: 321–327
DOI 10.1007/s00249-003-0347-2

ARTICLE

C. Terryn · J. Michel · X. Thomas · D. Laurent-Maquin
G. Balossier

Implementation of subcellular water mapping by electron energy loss spectroscopy in a medium-voltage scanning transmission electron microscope

Received: 10 March 2003 / Revised: 1 July 2003 / Accepted: 19 July 2003 / Published online: 3 September 2003

Abstract The water concentration in biological cells plays a predominant role in cellular life. Using electron energy loss spectroscopy, the feasibility to measure the water content in cells has already been demonstrated. In this paper, we present an upgrade of water measurement in hydrated cryosections by spectrum imaging mode in a medium-voltage scanning transmission electron microscope. The electron energy loss spectra are recorded in spectrum imaging mode in a $2^n \times 2^n$ pixels array. Each spectrum is processed in order to determine the water mass content in the corresponding pixel. Then a parametric image is obtained in which grey levels are related to water concentration. In this image, it is possible to recognize the different subcellular compartments. By averaging the water concentration over the relevant pixels, we can determine the water mass content in the concerned subcellular compartment. As an example, we present water mass content measurement at subcellular level in rat hepatocytes.

Keywords Cryomethods · Electron energy loss spectroscopy · Scanning transmission electron microscope · Spectrum imaging · Water content

Introduction

Water is an important and a major component of biological cells (Dubochet et al. 1987; Sun et al. 1995). Water is concerned in ionic flow regulation and in cellular volume regulation. Then the measurement of water content variations in the cell allows study of cellular life phenomena. Moreover, it is an important parameter to know while studying cell pathologies, especially those related to ionic or water channel failure.

Moreover, the knowledge of the water content can be coupled with elemental microanalysis by energy dispersive X-ray spectroscopy (EDXS) to express ionic concentrations in millimoles per litre (Gupta et al. 1978; Roomans 1988).

Other methods of water measurement at the subcellular level have been already published. We can cite three methods based on X-ray microanalysis. The first one is based on the differences in the continuum intensity between hydrated and freeze-dried cryosections (Gupta and Hall 1981; Saubermann et al. 1981; Zs-Nagy et al. 1982). This continuum intensity variation is assumed to be proportional to the specimen local mass variation and in that way this variation can be related to the water content. The second method takes into account the differences in the oxygen peak intensities before and after freeze-drying (Marshall 1980, 1987; Roomans 1988). The third method developed by Rick et al (1979; Warner 1986) on freeze-dried cryosections provides good sensitivity, but it requires a peripheral standard of known water content to be cryosectioned with the biological sample. Unfortunately, methods based on X-ray microanalysis require an important electron dose which can induce a considerable mass loss in the sensitive hydrated specimen.

Another method (Zierold 1986) uses the scanning transmission electron microscope (STEM) quantitative darkfield intensity on freeze-dried cryosections. In other work, a method developed by Hosoi et al (1981) and Leapman et al (1984) is based on the zero-loss peak attenuation between hydrated and freeze-dried cryosections in an electron energy loss spectroscopy (EELS) experiment. It is also possible to determine the water content by combining some of these methods (Von Zglinicki 1991).

C. Terryn (✉) · J. Michel · D. Laurent-Maquin · G. Balossier
Laboratoire de Microscopie Electronique Analytique,
INSERM ERM 0203, 21 rue Clément Ader,
51685 Cedex 2 Reims, France
E-mail: christine.terryn@univ-reims.fr
Tel.: +33-3-26050750
Fax: +33-3-26051900

X. Thomas
GSMA, UMR 6089, Faculté des Sciences,
BP 1039, 51687 Cedex 2 Reims, France

All the above-mentioned methods estimate the water content by using freeze-dried cryosections. Thereby they are indirect methods of local water measurement and are based on the assumption that no differential shrinkage occurs during freeze-drying.

A direct method of water mass measurement on hydrated cryosections has been developed by Sun et al (1993). It uses the fact that amorphous ice and macromolecular compounds exhibit specific spectral features in the low-loss part of electron energy loss spectra. This method has been implemented in our laboratory in a medium-voltage transmission electron microscope (TEM) (Terryn et al. 2000).

The aim of this paper is to present our upgrade of this method using a medium-voltage scanning transmission electron microscope (STEM). More precisely, the upgrade consists of implementation of water mass mapping in a spectrum imaging mode (Sun et al. 1995). Spectra are henceforth recorded for each pixel in a chosen area of the STEM image of the specimen. In this way, we have developed dedicated software to process the entire set of spectra of the studied area of the specimen. The water content is then obtained for each pixel and we can build up a water content map of the studied area of the specimen. As an example, we present the water mass content mapping at subcellular level in rat hepatocytes.

Materials and methods

Specimen preparation

The method of culturing and isolation of the rat hepatocytes is exactly described elsewhere (Petzinger et al. 1988; Zierold 1997). To summarize, hepatocytes are isolated from male Wistar rats by collagenase and then cultured in an incubator in modified Dulbecco's modified Eagle's medium at 5% carbon dioxide, 95% air atmosphere and 310 K on Petriperm dishes (Heraeus Instruments, Osterode, Germany). After formation of a confluent epithelium (1 day), discs of 2 cm in diameter are punched out from the Petriperm dish with attached cells, and spanned over a semi-sphere-like end of a Plexiglas rod of 2 mm diameter. These rods are then rapidly plunged in liquid ethane cooled by liquid nitrogen (Zierold 1997) for cryofixation. The frozen cells' monolayer is next cryosectioned at a nominal thickness of 70 nm by means of a FC 4E Reichert Jung ultracryomicrotome. The hydrated cryosections are placed onto Lacey films grids (AGAR, Essex, UK).

Analysis of the specimen

The hydrated cryosections were then transferred into the STEM (Philips CM 30) with a specimen cryoholder (GATAN, Pleasanton, USA). The observations were made in STEM mode using an accelerating voltage of 250 kV. The EELS experiments were performed with a GATAN PEELS 666 (Pleasanton, USA). The energy loss spectra were read from a 1D photodiode array as a series of one or many detector readouts. We used an energy dispersion of 0.1 eV per channel. The sensitivity of the photodiode is about one count per 22 impinging electrons for an accelerating voltage of 250 kV. A host computer interfaced with the microscope controlled the whole system. Dedicated acquisition software developed in our laboratory allowed control of the electron probe and the collection of the PEELS spectra in spectrum imaging mode.

Spectra acquisition in spectrum imaging mode

To obtain a water mass content map in hydrated cryosections, the EELS spectra are recorded in the spectrum imaging mode (Balossier et al. 1991; Hunt and Williams 1991; Colliex et al. 1994). While the electron probe scans a chosen specimen area, for each X and Y positions of the probe an EELS raw spectrum is recorded. The acquisition result is a data cube in which an entire EELS raw spectrum is stored for each X and Y position (Fig. 1). After processing of this data cube, parametric images related to EELS information can be built up.

In order to record a significant EELS signal, avoiding radiation damage in the hydrated specimen, we have to adjust the experimental parameters. The hydrated cryosections are very sensitive to damage created by electron beam irradiation. For an electron dose larger than approximately 1000 electrons/nm^2, a phenomenon called "bubbling" appears (formation of a hydrogen gas in the specimen), which is detected in the EELS spectrum (Fig. 2) by the hydrogen characteristic edge at 13.6 eV (Sun et al. 1995). To prevent this effect while recording a sufficient EELS signal, we adapted our experimental parameters in order to obtain an electron dose of approximately 500 electrons/nm^2. Using a 10-μm second condenser aperture in the electron microscope, we reduced the electron beam current at 0.1 nA. To obtain the best fitted electron dose, we also had to defocus the electron probe up to a 200 nm diameter and we chose an acquisition time per pixel of 0.1 s.

In a 64×64 pixels image, the electron probe scans a specimen area of 13 μm×13 μm. This area size is suitable to record the EELS signal of a whole biological cell, with a lateral resolution (200 nm) revealing the subcellular signal. The total acquisition time is approximately 7 min, allowing avoidance of significant specimen drift during the electron probe irradiation.

Correction of spectra energy shift during acquisition

During the probe scan, we observed an energy shift of the spectra. This is due to the optical coupling between the spectrometer and the microscope. Owing to the remnants of the photodiode array, this shift is responsible for an artefact in the spectrum. It appears as a "ghost" of the zero-loss peak from the previous recorded spectrum (Fig. 3). To remove this energy shift between successive spectra, we developed an acquisition system which allows control of the drift tube applied voltage in order to counteract this artefactual energy shift. This correction is not straightforward because this shift is not in a linear relationship with the displacement of the

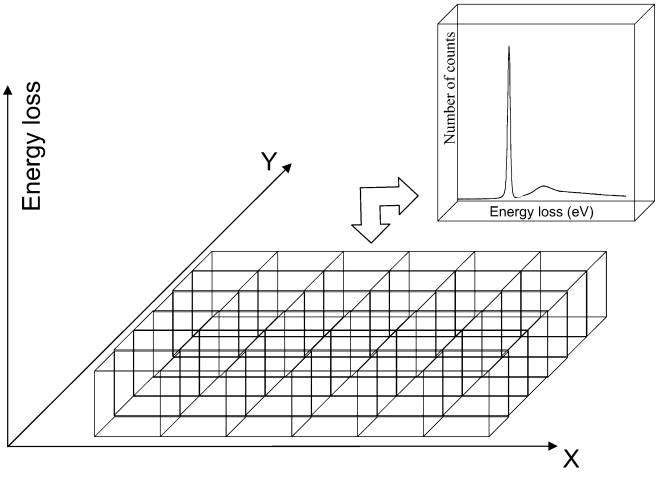

Fig. 1 Data cube containing EELS spectra recorded in spectrum imaging mode. For each (X, Y) position of the probe, an EELS raw spectrum is recorded

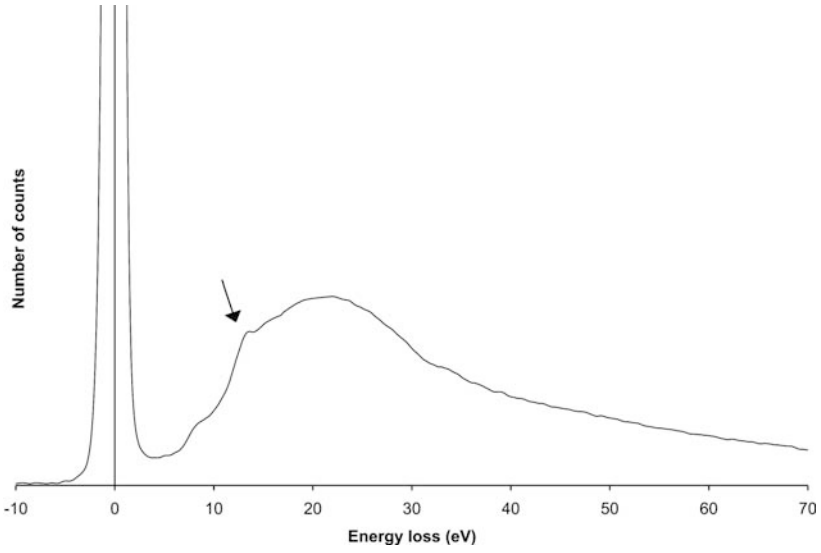

Fig. 2 "Bubbling" phenomenon: hydrogen characteristic edge at 13.6 eV

probe and it depends of the directions of the scan axes relative to the X and Y optical axes of the microscope column. The correction factors' determination has to be done for each spectrum imaging recording.

The shift counteractions which have to be applied on the drift tube for each (X,Y) position of the probe verify power laws depending on X, Y and XY values. Correction factors, C_X, C_Y and C_{XY}, are expressed as digital values in the software and correspond to calibrated voltages applied to the drift tube. They are calculated using the following equations:

$$C_X = A_X X^{B_X} \tag{1}$$

$$C_Y = A_Y Y^{B_Y} \tag{2}$$

$$C_{XY} = A_{XY}(XY)^{B_{XY}} \tag{3}$$

The A_X, B_X, A_Y, B_Y, A_{XY} and B_{XY} coefficients are experimentally determined. We use three points to determine the A_X and B_X coefficients: the first, the middle and the last points of the analysed area first line. We measure the corresponding energy shifts and then deduce the calibrated A_X and B_X coefficients. We proceed in the same way for the analysed area first column to determine the A_Y and B_Y coefficients and for the analysed area diagonal line to calculate the A_{XY} and B_{XY} coefficients. The final correction factor, C_K, is then calculated for each (X,Y) position by adding the three C_X, C_Y and C_{XY} coefficients. An example of the C_K values versus X and Y is presented in Fig. 4 for a 16×16 pixels map.

Processing of the electron energy loss spectra

Processing of each spectrum of the spectrum imaging acquisition file is performed using home-made software written in visual Basic whose organization chart is presented in Fig. 5. In a loop, for each (X,Y) spectrum we perform a full process of several steps operated sequentially: dark current removal, non-linearity correction (Egerton 1996), rejection of unsuitable spectra, precise energy calibration, point spread function deconvolution, Fourier-log deconvolution and finally weighted multiple least-squares fitting. When the specimen thickness is very important, the corresponding spectra cannot be processed by Fourier-log deconvolution and they are rejected in the loop and the water mass content is arbitrary fixed at zero. Energy calibration is performed for each spectrum by a maximum correlation coefficient computation. Indeed, any error in energy calibrating induces a significant change (a few percent) in the water mass measurement. This change is linear versus the miscalibration; Fig. 6 presents a typical variation of water measurement versus miscalibration. Thanks to the Fourier-log deconvolution

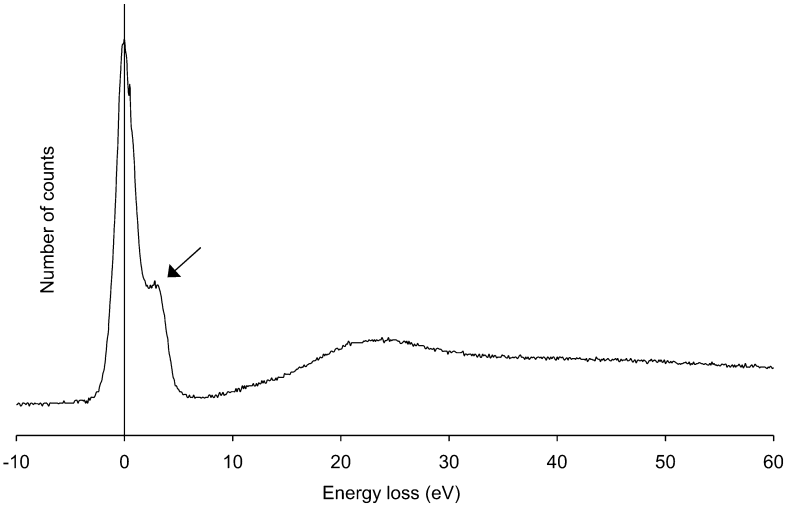

Fig. 3 Zero-loss peak remnant in the photodiode detector. This artefact is encountered when successive shifted energy loss spectra are recorded

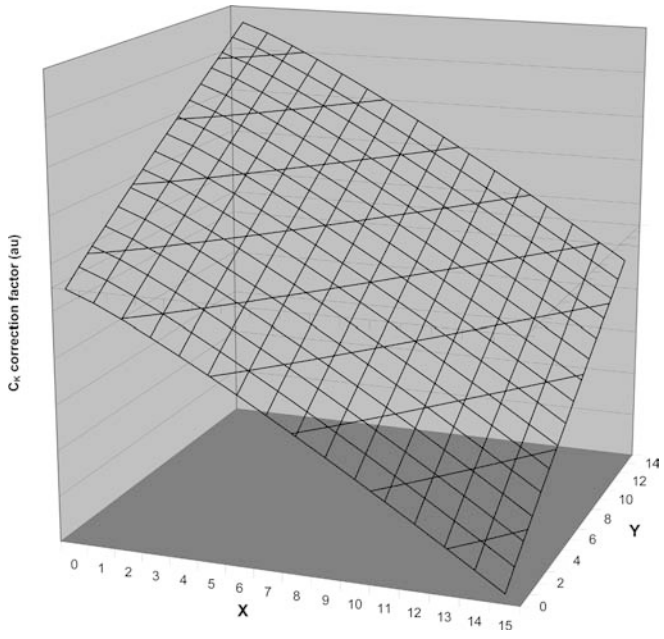

Fig. 4 Example of drift tube factor correction C_K versus X and Y positions of the electron probe for a 16×16 pixels map

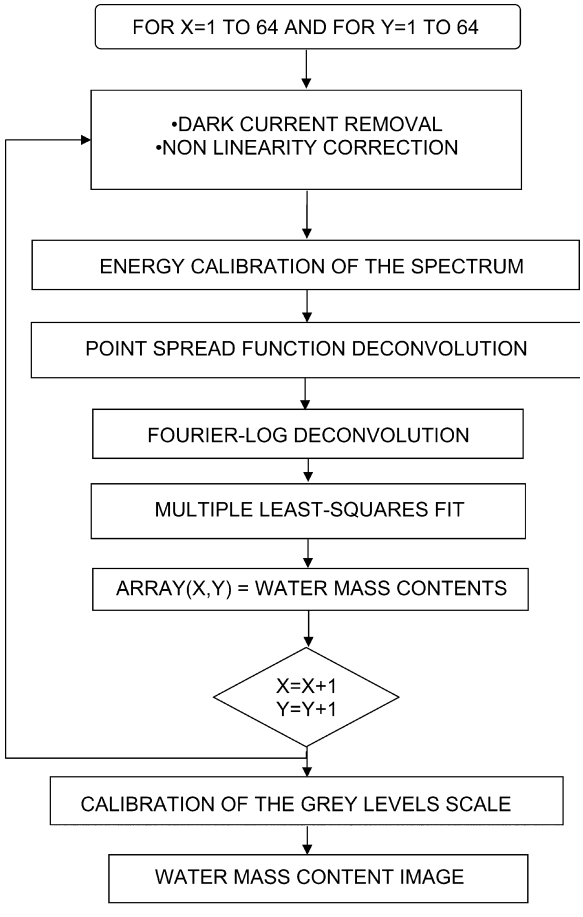

Fig. 5 Organization chart presenting the different steps of the spectrum processing

(Egerton 1982), the method is independent of the cryosection thickness variation. As a matter of fact, the single scattering distribution, $S(E)$, is given by the following equation:

$$S(E) = F^{-1}\left[I_0 \ln\left(\frac{(F(I(E))}{I_0}\right)\right] \tag{4}$$

where F and F^{-1} denote respectively the forward and the inverse Fourier transforms, I_0 is the zero loss peak intensity, and $I(E)$ is the measured intensity in the energy loss spectrum. Providing the cryosections are sufficiently thin, the method is potentially independent of the thickness.

The final step is the weighted multiple least-squares fitting. The basic principle is that the normalized single-scattering distribution from the hydrated specimen $S(E)$ can be expressed as a linear sum of the normalized single-scattering distributions $S_i(E)$ from its separate components:

$$S(E) = \sum_{i=1}^{M} a_i S_i(E) \tag{5}$$

Experimentally, the EELS spectra from different macromolecular compounds (protein, lipid, sugar, etc.) are very similar under our experimental conditions. We then assume, in a first approximation, that the single-scattering distribution of the hydrated specimen can be modelled by only two reference spectra: the ice single-scattering distribution, $S_{\text{water}}(E)$, and the protein (BSA) reference single scattering distribution, $S_{\text{prot}}(E)$. In addition, the cryosections are placed onto network-like (lacey) support films, which avoids film correction requirement. Then the single scattering of the specimen is modelled by:

$$S(E) = a_{\text{water}} S_{\text{water}}(E) + a_{\text{prot}} S_{\text{prot}}(E) \tag{6}$$

The coefficients a_{water} and a_{prot} are obtained by a multiple least-squares fitting procedure (Bevington 1969), in which we minimize the χ^2 value defined by:

$$\chi^2 = (cI_{\text{tot}})^2 \times \sum_{n=1}^{N} \frac{\left[S(E_n) - a_{\text{water}} S_{\text{water}}(E_n) - a_{\text{prot}} S_{\text{prot}}(E_n)\right]^2}{\left(\frac{cI(E_n)}{DQE}\right)} \tag{7}$$

where $c = 22$ is the conversion factor for the number of primary electrons per photodiode count and $DQE = 0.1$ is the detection quantum efficiency of the detector for our typical number of counts per channel.

The mass fraction of water, l, can then be expressed by (see Terryn et al. 2000 for derivation details):

$$l = \frac{\frac{a_{\text{water}}}{(\sigma/m)_{\text{water}}}}{\frac{a_{\text{water}}}{(\sigma/m)_{\text{water}}} + \frac{a_{\text{prot}}}{(\sigma/m)_{\text{prot}}}} \tag{8}$$

where $(\sigma/\text{m})_{\text{water}}$ and $(\sigma/\text{m})_{\text{prot}}$ are the mass cross-section of water and protein, which are experimentally determined (Sun et al. 1993; Terryn et al. 2000).

The whole procedure is applied to each spectrum of the data cube and finally we build up a parametric image in which grey levels correspond to the water mass content. The grey level scale can be optimized in order to enhance the image contrast. It is also possible to add up pixels in a chosen cell compartment to obtain the average water mass content. With a PC including a 600 MHz processor and 160 Mb RAM, typical maps corresponding to 64×64 spectra are processed in 20 min.

Relative thickness map

Using the recorded EELS spectrum, it is also possible to obtain the relative specimen thickness, t/λ, where λ is the inelastic mean free path, by the following equation:

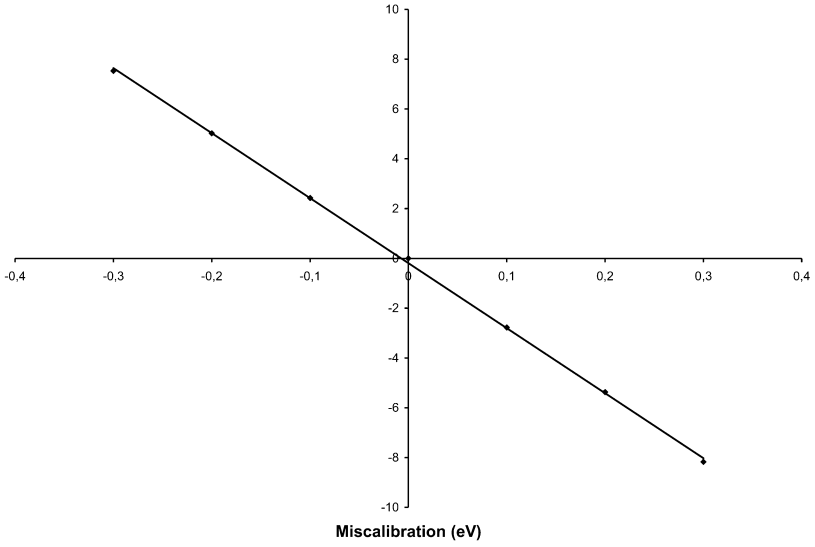

Fig. 6 Variation of the water mass content measurement versus the miscalibration

$$\frac{t}{\lambda} = \ln\left(\frac{I_{\text{tot}}}{I_0}\right) \tag{9}$$

where I_0 is the zero loss peak intensity and I_{tot} corresponds to the summation of the spectrum intensities over all energy losses. Owing to the spectra energy range limitation, we have to extend spectra up to higher energy loss values using a AE^{-r} power law dependence. By applying this process to the data cube, we then build up the relative thickness map of the studied specimen area.

Results

The test sample is a cryosection of rat hepatocytes. In this frozen hydrated specimen, observed at a temperature of −175 °C, we recorded a 64×64 pixels map with a probe size of 200 nm and an electron dose of 500 e^-/nm^2. Then after freeze-drying the specimen, we recorded the corresponding inverse darkfield image (Fig. 7a). With the spectrum imaging data set, we built up the relative thickness map (Fig. 7b) and the parametric image where the grey levels correspond to the water mass content (Fig. 7c), as explained in the previous section.

It is possible to make some area correspondence between the frozen hydrated relative thickness map and the freeze-dried darkfield image of the cryosection. We use the lacey film network to recognize specimen areas. The square boxes in Fig. 7a and Fig. 7b correspond to similar areas.

A good illustration is a spurious ice crystal on top of the hydrated specimen. In the relative thickness map, we can see a dark region (see arrow in the Fig. 7b) corresponding to a high relative thickness region. In the water mass content image, this region corresponds as expected to a region with approximately 100% water mass content.

In order to obtain an optimized contrast and since water mass concentrations are always higher than 50%, we used a scale varying from 50% water mass concentration (black level) to 100% water mass concentration (white level). In the water mass content map we can then recognize the different subcellular compartments: nucleus, cytoplasm and mitochondria. To determine the water mass content in each compartment, we averaged the water percentages over 10 or 20 pixels in the relevant areas, avoiding the pixels corresponding to the lacey film. In this way, we used the correspondence of the pixels between the relative thickness map and the water mass content image.

From the analysis of 10 hepatocytes cryosections, we determined that the water mass concentrations were

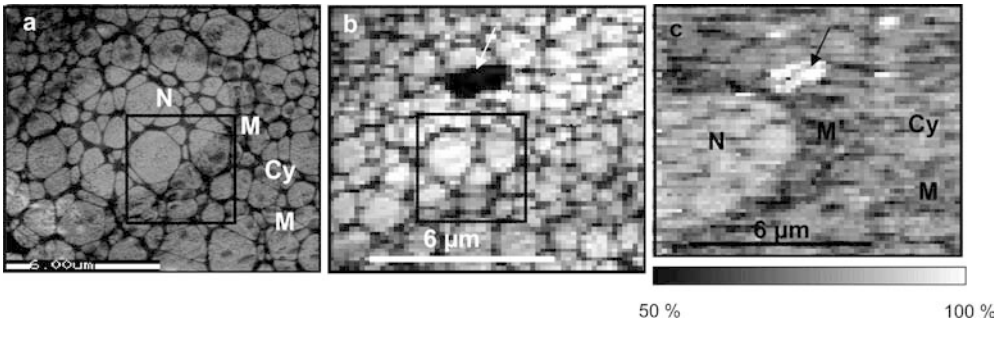

Fig. 7 (**a**) Inverse darkfield image of the freeze-dried rat hepatocyte cryosection. (**b**) Corresponding relative mass thickness map of the frozen hydrated cryosection. (**c**) Corresponding parametric image of water mass content in the cryosection. The *arrow* shows the ice crystal. The *square boxes* correspond to similar areas in (**a**) and (**b**). N = nucleus, Cy = cytoplasm, M = mitochondria

$88 \pm 3\%$ for the nucleus, $76 \pm 1\%$ for the cytoplasm and $65 \pm 3\%$ for mitochondria (Table 1).

Discussion and conclusion

The water mass contents measured in rat hepatocytes are larger than those found in the literature for the darkfield method (Bolkent and Zierold 2002), particularly in mitochondria. A first explanation of this discrepancy could be related to the apparition of a hydration shell on the frozen hydrated cryosections. However, it has been demonstrated on standard specimen cryosections (Sun et al. 1993; Terryn et al. 2000) that this phenomenon is negligible provided sufficient care is taken during the specimen preparation. The origin of this discrepancy could also be explained, in the darkfield method, by differential lateral shrinkage between the specimen and the standard during freeze-drying. As a matter of fact, if the lateral shrinkage is more important in biological cryosection than in the standard cryosection, the dry weight percentage could be overestimated, inducing a lowered water mass content.

Compared to others methods, EELS allows us to obtain a direct measurement of the water content on a hydrated cryosection. It is possible to study water mass concentration variations in physiological cells with a good lateral resolution (200 nm in our experiment). However, two problems appear when we want to study hydrated frozen cryosections. The first one is the high specimen sensitivity to electron beam irradiation. In order to avoid significant radiation damage, we optimized our analysis conditions. In this way, in our experimental conditions we used an electron probe diameter of 200 nm. This probe size, defining the resolution, is a good compromise between a relevant EELS signal detection and an electron dose ($500\ e^-/nm^2$) which induced no significant irradiation damage in the specimen. This lateral resolution could be reduced up to a few tens of nanometers at the detriment of the measurement precision, owing to the weak recorded signal. In this way, improvement of the recording system (CCD detector with better DQE for low count experiments) will permit us to improve the lateral resolution of the method. We recorded three consecutive measurements of the water content in the same specimen area with this chosen electron dose and we observed a water mass percentage variation between the first and the last measurement lower than 1%.

The second problem is the very low contrast in hydrated cryosections. Implementation in the spectrum imaging mode allows us to overcome this problem. Thanks to the relative thickness map, it is possible to correlate the water mass content image and the freeze-dried darkfield image. In this way, the use of lacey film presents two advantages. Firstly, the recorded energy loss signal does not contain any spurious signal due to the support film. This fact simplifies the spectra processing because we do not have to take into account the signal of the support film. Secondly, from a practical point of view, it becomes possible to record several water maps in different areas of a frozen hydrated specimen since it is possible to recognize these chosen areas in the freeze-dried darkfield image using the particular features of the lacey support film.

Instead of a 64×64 pixels image, it is, of course, possible to record an image with a larger or a smaller number of pixels. The spectrum imaging acquisition and processing are just more or less time-consuming.

This method using EELS allows us to determine water mass content in hydrated biological cryosections in a direct way. Then, the possible artefacts related to freeze-drying are avoided by this approach. The Fourier-log deconvolution allows the method to be independent of the thickness variations of the cryosections. The implementation of the technique in spectrum imaging mode facilitates the results exploitation. Moreover, we can average the water concentration in several pixels of a chosen subcellular compartment.

From an experimental point of view, this method could take benefit of technological improvements concerning the energy resolution (with a field emission gun), the dynamics and the DQE of the recording system (CCD detector for example).

By coupling this method with X-rays microanalysis, we will be able to express the ionic concentrations in millimoles per litre. The subcellular water mapping by EELS provides us a powerful tool to study pathologies or cellular life phenomena.

Acknowledgements The authors thank Dr. Karl Zierold (Max Planck Institut für Molekular Physiology, Dortmund, Germany) for his precious advice on cryomethods and for helpful discussions.

Table 1 Water mass content measured in different subcellular compartments of rat hepatocyte cryosections[a]

Subcellular compartments	Measured water mass content (%)	Literature (Bolkent and Zierold 2002)
Nucleus	88 ± 3	75 ± 8
Cytoplasm	76 ± 1	70 ± 5
Mitochondria	65 ± 3	50 ± 5

[a]Mean percentage ± standard deviation calculated on 10 cryosections

References

Balossier G, Thomas X, Michel J, Wagner D, Bonhomme P, Puchelle E, Ploton D, Bonhomme A, Pinon JM (1991) Parallel EELS elemental mapping in scanning transmission electron microscopy: use of the difference methods. Microsc Microanal Microstruct 2:531–546

Bevington PR (1969) Data reduction and error analysis for the physical sciences. McGraw-Hill, New York

Bolkent S, Zierold K (2002) Effects of the ionophores valinomycin, ionomycin and gramicidin A on the element compartmentation in cultured rat hepatocytes. Toxicol In Vitro 16:159–165

Colliex C, Tence M, Lefevre E, Mory C, Huigu D, Bouchet D, Jeanguillaume C (1994) Electron energy loss spectrometry mapping. Mikrochim Acta 114–115:71–87

Dubochet J, Adrian M, Chang JJ, Lepault J, McDowall AW (1987) Cryoelectron microscopy of vitrified specimen. In: Steinbrecht RA, Zierold K (eds) Cryotechniques in biological electron microscopy. Springer, Berlin Heidelberg New York, pp 114–118

Egerton RF (1982) Thickness dependence of the STEM ratio image. Ultramicroscopy 10:297–299

Egerton RF (1996) Electron energy loss spectroscopy in the electron microscope, 2nd edn. Plenum Press, New York

Gupta BL, Hall TA (1981) The X-ray microanalysis of frozen-hydrated sections in scanning electron microscopy: an evaluation. Tissue Cell 13:623–643

Gupta BL, Berridge MJ, Hall TA, Moreton RB (1978) Electron microprobe and ion-selective microelectrode studies of fluid secretion in the salivary glands of Calliphora. J Exp Biol 72:261–284

Hosoi J, Oikawa T, Inoue M, Kokubo Y, Hama K (1981) Measurement of partial specific thickness (net thickness) of critical-point-dried cultured fibroblast by energy analysis. Ultramicroscopy 7:147–154

Hunt JA, Williams DB (1991) Electron energy loss spectrum-imaging. Ultramicroscopy 38:47–73

Leapman RD, Fiori CE, Swyt CR (1984) Mass thickness determination by electron energy loss for quantitative X-ray microanalysis in biology. J Microsc 133:239–253

Marshall AT (1980) Quantitative x-ray microanalysis of frozen-hydrated bulk biological specimens. Scanning Electron Microsc 2:335–348

Marshall AT (1987) Scanning electron microscopy and X-ray microanalysis of frozen-hydrated bulk samples. In Steinbrecht RA, Zierold K (eds) Cryotechniques in biological electron microscopy. Springer, Berlin Heidelberg New York

Petzinger E, Föllmann W, Acker H, Hentschel J, Zierold K, Kinne RKH (1988) Primary liver cell cultures grown on gas permeable membrane as source for the collection of primary bile. In Vitro Cell Dev Biol 24:491–499

Rick R, Dörge A, Gehring R, Bauer R, Thureau K (1979) Quantitative determination of cellular electrolyte concentrations in thin freeze-dried cryosections using energy dispersive X-ray microanalysis. In: Lechene CP, Warner RR (eds) Microbeam analysis in biology. Academic Press, New York

Roomans GM (1988) Quantitative X-ray microanalysis of biological specimens. J Electron Microsc Tech 9:19–43

Saubermann AJ, Beeuwkes R III, Peters PD (1981) Application of scanning electron microscopy to x-ray analysis of frozen-hydrated sections. II. Analysis of standard solutions and artificial electrolyte gradients. J Cell Biol 88:268–273

Sun SQ, Shi SL, Leapman RD (1993) Water distributions of hydrated biological specimens by valence electron energy loss spectroscopy. Ultramicroscopy 50:127–139

Sun SQ, Shi SL, Hunt J, Leapman RD (1995) Quantitative water mapping of cryosectioned cells by electron energy loss spectroscopy. J Microsc 177:18–30

Terryn C, Michel J, Kilian L, Bonhomme P, Balossier G (2000) Comparison of intracellular water content measurements by dark-field imaging and EELS in medium voltage TEM. Eur Phys J AP 11:215–226

Von Zglinicki T (1991) The measurement of water distribution in frozen specimen. J Microsc 161:149–158

Warner RR (1986) Water content from analysis of freeze-dried thin sections. J Microsc 142:363–369

Zierold K (1986) The determination of wet weight concentrations of elements in freeze-dried cryosections from biological cells. Scanning Electron Microsc 2:713–724

Zierold K (1997) Effects of cadmium on electrolyte ions in cultured rat hepatocytes studied by X-ray microanalysis of cryosections. Toxicol Appl Pharmacol 144:70–76

Zs-Nagy I, Lustyik G, Bertoni-Freddari C (1982) Intracellular water and dry mass content as measured in bulk specimens by energy-dispersive X-ray microanalysis. Tissue Cell 14:47–60